Inorg. Chem. **2007**, *46*, 9558–9568

Thermally Induced Two-Step, Two-Site Incomplete $^6A_1 \leftrightarrow {}^2T_2$ Crossover in a Mononuclear Iron(III) Phenolate–Pyridyl Schiff-Base Complex: A Rare Crystallographic Observation of the Coexistence of Pure $S = {}^5/_2$ and ${}^1/_2$ Metal Centers in the Asymmetric Unit

Musa S. Shongwe,*,† Badria A. Al-Rashdi,† Harry Adams,‡ Michael J. Morris,*,‡ Masahiro Mikuriya,*,§ and Giovanni R. Hearne||

Department of Chemistry, College of Science, Sultan Qaboos University, P.O. Box 36, Al-Khod 123, Muscat, Sultanate of Oman, Department of Chemistry, The University of Sheffield, Sheffield S3 7HF, United Kingdom, Department of Chemistry and Open Research Center for Molecule-Based Devices, School of Science and Technology, Kwansei Gakuin University, 2-1 Gakuen, Sanda 669-1337, Japan, and School of Physics, University of the Witwatersrand, Private Bag 3, Wits 2050, Johannesburg, South Africa

Received March 1, 2007

The six-coordinate mononuclear iron(III) complexes $[Fe(salpm)_2]ClO_4 \cdot 0.5EtOH$, $[Fe(salpm)_2]Cl$, $[Fe\{(3,5\text{-}{}^tBu_2)\text{-}salpm\}_2]X$ ($X = ClO_4^-$ or Cl^-), and $[Fe\{(3,5\text{-}{}^tBu_2)\text{-}salpm\}_2]NO_3 \cdot 2H_2O$ [Hsalpm = *N*-(pyridin-2-ylmethyl)-salicylideneamine; H(3,5-^{t}Bu$_2$)-salpm = *N*-(pyridin-2-ylmethyl)-3,5-di-*tert*-butylsalicylideneamine] have been synthesized and isolated in crystalline form; their chemical identities have been ascertained by elemental analyses, FAB mass spectrometry, and infrared spectroscopy. The room-temperature effective magnetic moments $[(8\chi_M T)^{1/2} \sim 5.85\text{–}5.90\ \mu_B]$ of these complexes are consistent with the high-spin ($S = {}^5/_2$) ground state. These complexes are intensely colored on account of the strong $p_\pi \rightarrow d_\pi^*$ LMCT visible absorptions. Definitive evidence for the structures of $[Fe(salpm)_2]ClO_4 \cdot 0.5EtOH$ and $[Fe\{(3,5\text{-}{}^tBu_2)\text{-}salpm\}_2]NO_3 \cdot 2H_2O$ has been provided by single-crystal X-ray crystallography. The monomeric complex cations in both compounds comprise two uninegative phenolate–pyridyl tridentate Schiff-base ligands coordinated meridionally to the iron(III) to afford a distorted octahedral geometry with a *trans,cis,cis*-$[FeO_2N_4]$ core. Whereas $[Fe(salpm)_2]ClO_4 \cdot 0.5EtOH$ undergoes a thermally induced $^6A_1 \leftrightarrow {}^2T_2$ crossover, $[Fe\{(3,5\text{-}{}^tBu_2)\text{-}salpm\}_2]NO_3 \cdot 2H_2O$ retains its spin state in the solid state down to 5 K. However, EPR spectroscopy reveals that the latter complex does exhibit a spin transformation in solution, albeit to a much lesser extent than does the former. The spin crossover in $[Fe(salpm)_2]ClO_4 \cdot 0.5EtOH$ has resulted in an unprecedented crystallographic observation of the coexistence of high-spin and low-spin iron(III) complex cations in equal proportions around 100 K. At room temperature, the two crystallographically distinct ferric centers are both high spin; however, one $[Fe(salpm)_2]^+$ complex cation undergoes a complete spin transition over the temperature range ~200–100 K, whereas the other converts very nearly completely between 100 and 65 K; ~10% of the complex cations in $[Fe(salpm)_2]ClO_4 \cdot 0.5EtOH$ remain in the high-spin state down to 5 K.

Introduction

Designing and synthesizing spin-crossover molecular materials is an exciting field of vigorous research endeavors driven largely by the recognition of the potential technological applicability of these electronically bistable substances as materials for information storage, molecular switches, and visual displays in molecule-based electronics.[1] Over the

* To whom correspondence should be addressed. E-mail: musa@squ.edu.om (M.S.S.), m.morris@sheffield.ac.uk (M.J.M.), junpei@ksc.kwansei.ac.jp (M.M.).
† Sultan Qaboos University.
‡ The University of Sheffield.
§ Kwansei Gakuin University.
|| University of the Witwatersrand.

(1) (a) Gütlich, P.; Hauser, A.; Spiering, H. *Angew. Chem., Int. Ed. Engl.* **1994**, *33*, 2024. (b) Real, J. A.; Andres, E.; Muñoz, M. C.; Julve, M.; Granier, T.; Bousseksou, A.; Varret, F. *Science* **1995**, *268*, 265. (c) Kahn, O.; Martinez, C. J. *Science* **1998**, *279*, 44. (d) Gütlich, P.; Garcia, Y.; Goodwin, H. A. *Chem. Soc. Rev.* **2000**, *29*, 418.

10.1021/ic700397u CCC: $37.00
Published on Web 10/05/2007

years, a diverse range of pseudo-octahedral $3d^n$ ($4 \leq n \leq 7$) spin-crossover systems have been reported,[1,2] for instance, d^4 (Mn^{III}: $S = 2 \leftrightarrow S = 1$[3]), d^5 (Fe^{III}: $S = {}^5/_2 \leftrightarrow S = {}^1/_2$;[4] $S = {}^5/_2 \leftrightarrow S = {}^3/_2$;[5] $S = {}^3/_2 \leftrightarrow S = {}^1/_2$[6]), d^6 (Fe^{II}: $S = 2 \leftrightarrow S = 0$[2d]), d^7 (Co^{II}: $S = {}^3/_2 \leftrightarrow S = {}^1/_2$[7]).

The crucial criterion for a spin transition to occur is that the ligand-field splitting parameter (Δ_o) should be very nearly equal to the spin-pairing energy (P).[2c,8] Thus, the spin state is sensitive to external perturbations; systematic studies of various spin-crossover systems involving variable-temperature magnetic susceptibility measurements, Mössbauer spectroscopy, EPR spectroscopy, and X-ray crystallography have revealed that spin transitions can be induced, inter alia, by temperature,[1−9] irradiation,[10] pressure,[11] counterions,[10c,12] the nature and positions of substituent groups on phenolic[13a] or pyridyl[13b,c] rings, lattice solvents,[14] and the type of sample (i.e., crystalline or powder).[7,14b,15] The discovery of the Light-Induced Excited Spin-State Trapping effect by Decurtins et al.[16] has aroused further interest in spin crossovers, raising the possibility that optically switchable bistable materials can find applications in the fabrication of optical devices. It has been amply demonstrated that spin crossovers exhibit multifarious forms; for instance, they can be abrupt,[15c,17] gradual,[7,12a,d,14b,15a,b,18] discontinuous with hysteresis,[4a,b,9c,10b−e,15c] two-step,[4a,15c] incomplete,[12,18,19] irreversible,[12e] or accompanied by a structural phase transition.[20]

The spin-crossover phenomenon is also pursued with great interest in bioinorganic chemistry as it can be employed to illuminate the causes of spin-state conversions in iron-based biological systems involving both heme and non-heme metalloproteins. In heme proteins, the mode of interaction of the porphyrin ring with iron depends on the oxidation state and spin state of iron and influences the overall function of the biomolecule in question. Porphyrin complexes of iron(II) and iron(III) often have coordination environments that favor a spin crossover involving the intermediate spin state.[6,21] The spin-crossover phenomenon can also provide insight into the factors that govern the spin state of non-heme Fe^{III}−OOH species in oxidative catalysis (e.g., activated bleomycin).[22] Furthermore, it can help shed light on the unusual $S = {}^3/_2$ ground states exhibited by nitrosyl (NO)

(2) (a) Goodwin, H. A. *Coord. Chem. Rev.* **1976**, *18*, 293. (b) Nelson, S. M. Iron(III) and Higher States In *Comprehensive Coordination Chemistry*; Wilkinson, G., Gillard, R. D., McCleverty, J. A., Eds.; Pergamon Books Ltd: Oxford, 1987; pp 217−276. (c) Cotton, F. A.; Wilkinson, G.; Murillo, C. A.; Bochmann, M. *Advanced Inorganic Chemistry*, 6th Edition; John Wiley & Sons: New York, 1999; pp 785−786. (d) Real, J. A.; Gaspar, A. B.; Niel, V.; Muñoz, C. M. *Coord. Chem. Rev.* **2003**, *236*, 121. (e) Sunatsuki, Y.; Ikuta, Y.; Matsumoto, N.; Ohta, H.; Kojima, M.; Iijima, S.; Hayami, S.; Maeda, Y.; Kaizaki, S.; Dahan, F.; Tuchagues, J.-P. *Angew. Chem., Int. Ed.* **2003**, *42*, 1614.

(3) (a) Sim, P. G.; Sinn, E. *J. Am. Chem. Soc.* **1981**, *103*, 241. (b) Garcia, Y.; Kahn, O.; Ader, J.-P.; Buzdin, A.; Meurdesoif, Y.; Guillot, M. *Phys. Lett. A* **2000**, *271*, 145. (c) Guionneau, P.; Marchivie, M.; Garcia, Y.; Howard, J. A. K.; Chasseau, D. *Phys. Rev. B* **2005**, *72*, 214408.

(4) (a) Hayami, S.; Gu, Z.; Yoshiki, H.; Fujishima, A.; Sato, O. *J. Am. Chem. Soc.* **2001**, *123*, 11644. (b) Dorbes, S.; Valade, L.; Real, J. A.; Faulmann, V. *Chem. Commun.* **2005**, 69.

(5) Butcher, R. J.; Ferraro, J. R.; Sinn, E. *J. Chem. Soc., Chem. Commun.* **1976**, 910.

(6) (a) Wells, F. V.; McCann, S. W.; Wickman, H. H.; Kessel, S. L.; Hendrickson, D. N.; Feltham, R. D. *Inorg. Chem.* **1982**, *21*, 2306. (b) König, E.; Ritter, G.; Dengler, J.; Larkworthy, L. F. *Inorg. Chem.* **1992**, *31*, 1196. (c) Koch, W. O.; Schünemann, V.; Gerdan, M.; Trautwein, A. X.; Krüger, H.-J. *Chem.−Eur. J.* **1998**, *4*, 686. (d) Ikeue, T.; Ohgo, Y.; Yamaguchi, T.; Takahashi, M.; Takeda, M.; Nakamura, M. *Angew. Chem., Int. Ed.* **2001**, *40*, 2617. (e) Ohgo, Y.; Ikeue, T.; Nakamura, M. *Inorg. Chem.* **2002**, *41*, 1698. (f) Li, M.; Bonnet, D.; Bill, E.; Neese, F.; Weyhermüller, T.; Blum, N.; Sellmann, D.; Wieghardt, K. *Inorg. Chem.* **2002**, *41*, 3444.

(7) (a) Faus, J.; Julve, M.; Lloret, F.; Real, J. A.; Sletten, J. *Inorg. Chem.* **1994**, *33*, 5535. (b) Sieber, R.; Decurtins, S.; Stoeckli-Evans, H.; Wilson, C.; Yufit, D.; Howard, J. A. K.; Capelli, S. C.; Hauser, A. *Chem.−Eur J.* **2000**, *6*, 361.

(8) Huheey, J. E.; Keiter, E. A.; Keiter, R. L. *Inorganic Chemistry: Principles of Structure and Reactivity*, 4th Edition; Harper Collins College Publishers: New York, 1993; pp 464−466.

(9) (a) Holland, J. M.; McAllister, J. A.; Lu, Z.; Kilner, C. A.; Thornton-Pett, M.; Halcrow, M. A. *Chem. Commun.* **2001**, 577. (b) Hayami, S.; Kawajiri, R.; Juhász, G.; Kawahara, T.; Hashiguchi, K.; Sato, O.; Inoue, K.; Maeda, Y. *Bull. Chem. Soc. Jpn.* **2003**, *76*, 1207. (c) Boča, R.; Renz, F.; Boča, M.; Fuess, H.; Haase, W.; Kickelbick, G.; Linert, W.; Vrbová-Schikora, M. *Inorg. Chem. Commun.* **2005**, *8*, 227. (d) Tanimura, K.; Kitashima, R.; Bréfuel, N.; Nakamura, M.; Matsumoto, N.; Shova, S.; Tuchagues, J.-P. *Bull. Chem. Soc. Jpn.* **2005**, *78*, 1279.

(10) (a) Breuning, E.; Ruben, M.; Lehn, J.-M.; Renz, F.; Garcia, Y.; Ksenofontov, V.; Gütlich, P.; Wegelius, E.; Rissanen, K. *Angew. Chem., Int. Ed.* **2000**, *39*, 2504. (b) Hayami, S.; Gu, Z.; Shiro, M.; Einaga, Y.; Fujishima, A.; Sato, O. *J. Am. Chem. Soc.* **2000**, *122*, 7126. (c) Juhász, G.; Hayami, S.; Sato, O.; Maeda, Y. *Chem. Phys. Lett.* **2002**, *364*, 164. (d) Freysz, E.; Montant, S.; Létard, S.; Létard, J.-F. *Chem. Phys. Lett.* **2004**, *394*, 318. (e) Bonhommeau, S.; Molnár, G.; Galet, A.; Zwick, A.; Real, J. A.; McGarvey, J. J.; Bousseksou, A. *Angew. Chem., Int. Ed.* **2005**, *44*, 4069.

(11) (a) Sunatsuki, Y.; Sakata, M.; Matsuzaki, S.; Matsumoto, N.; M. Kojima *Chem. Lett.* **2001**, 1254. (b) Ksenofontov, V.; Gaspar, A. B.; Levchenko, G.; Fitzsimmons, B.; Gütlich, P. *J. Phys. Chem. B* **2004**, *108*, 7723. (c) Gaspar, A. B.; Agustí, G.; Martínez, V.; Muñoz, M. C.; Levchenko, G.; Real, J. A. *Inorg. Chim. Acta* **2005**, *358*, 4089.

(12) (a) Maeda, Y.; Tsutsumi, N.; Takashima, Y. *Inorg. Chem.* **1984**, *23*, 2440. (b) Timken, M. D.; Abdel-Mawgoud, A. M.; Hendrickson, D. N. *Inorg. Chem.* **1986**, *25*, 160. (c) Kennedy, B. J.; McGrath, A. C.; Murray, K. S.; Skelton, B. W.; White, A. H. *Inorg. Chem.* **1987**, *26*, 483. (d) Nishida, Y.; Kino, K.; Kida, S. *J. Chem. Soc., Dalton Trans.* **1987**, 1957. (e) Holland, J. M.; McAllister, J. A.; Kilner, C. A.; Thornton-Pett, M.; Bridgeman, A. J.; Halcrow, M. A. *J. Chem. Soc., Dalton Trans.* **2002**, 548.

(13) (a) Sim, P. G.; Sinn, E.; Petty, R. H.; Merrill, C. L.; Wilson, L. J. *Inorg. Chem.* **1981**, *20*, 1213. (b) Zang, Y.; Kim, J.; Dong, Y.; Wilkinson, E. C.; Appelman, E. H.; Que, L., Jr. *J. Am. Chem. Soc.* **1997**, *119*, 4197. (c) Hitomi, Y.; Higuchi, M.; Minami, H.; Tanaka, T.; Funabiki, T. *Chem. Commun.* **2005**, 1758.

(14) Selected examples: (a) Summerton, A. P.; Diamantis, A. A.; Snow, M. R. *Inorg. Chim. Acta* **1978**, *27*, 123. (b) Conti, A. J.; Chadha, R. J.; Sena, K. M.; Rheingold, A. L.; Hendrickson, D. N. *Inorg. Chem.* **1993**, *32*, 2670.

(15) (a) Hendrickson, D. N.; Haddad, M. S.; Federer, W. D.; Lynch, M. W. *Coord. Chem.* **1980**, *21*, 75. (b) Timken, M. D.; Hendrickson, D. N.; Sinn, E. *Inorg. Chem.* **1985**, *24*, 3947. (c) Reger, D. L.; Little, C. A.; Smith, M. D.; Rheingold, A. L.; Lam, K.-C.; Concolino, T. L.; Long, G. J.; Hermann, R. P.; Grandjean, F.; *Eur. J. Inorg. Chem.* **2002**, 1190.

(16) (a) Decurtins, S.; Gütlich, P.; Köhler, C. P.; Spiering, H.; Hauser, A. *Chem. Phys. Lett.* **1984**, *105*, 1. (b) Decurtins, S.; Gütlich, P.; Hasselbach, K. M.; Hauser, A.; Spiering, H. *Inorg. Chem.* **1985**, *24*, 2174.

(17) Sugiyarto, K. H.; McHale, W.-A.; Craig, D. C.; Rae, A. D.; Scudder, M. L.; Goodwin, H. A. *J. Chem. Soc., Dalton Trans.* **2003**, 2443.

(18) Singh, S.; Mishra, V.; Mukherjee, J.; Seethalekshmi, N.; Mukherjee, R. *Dalton Trans.* **2003**, 3392.

(19) Roelfes, G.; Lubben, M.; Chen, K.; Ho, R. Y. N.; Meetsma, A.; Genseberger, S.; Hermant, R. M.; Hage, R.; Mandal, S. K.; Young, V. G., Jr.; Zang, Y.; Kooijman, H.; Spek, A. L.; Que, L., Jr.; Feringa, B. L. *Inorg. Chem.* **1999**, *38*, 1929.

(20) (a) Conti, A. J.; Kaji, K.; Nagano, Y.; Sena, K. M.; Yumoto, Y.; Chadha, R. J.; Rheingold, A. L.; Sorai, M.; Hendrickson, D. N. *Inorg. Chem.* **1993**, *32*, 2681. (b) Hayami, S.; Shigeyoshi, Y.; Akita, M.; Inoue, K.; Kato, K.; Osaka, K.; Takata, M.; Kawajiri, R.; Mitani, T.; Maeda, Y. *Angew. Chem., Int. Ed.* **2005**, *44*, 4899.

(21) Scheidt, W. R.; Reed, C. A. *Chem. Rev.* **1981**, *81*, 543.

(22) (a) Stubbe, J.; Kozarich, J. W.; Wu, W.; Vanderwall, D. E. *Acc. Chem. Res.* **1996**, *29*, 322. (b) Sam, J. W.; Tang, X. J.; Peisach, J. *J. Am. Chem. Soc.* **1994**, *116*, 5250.

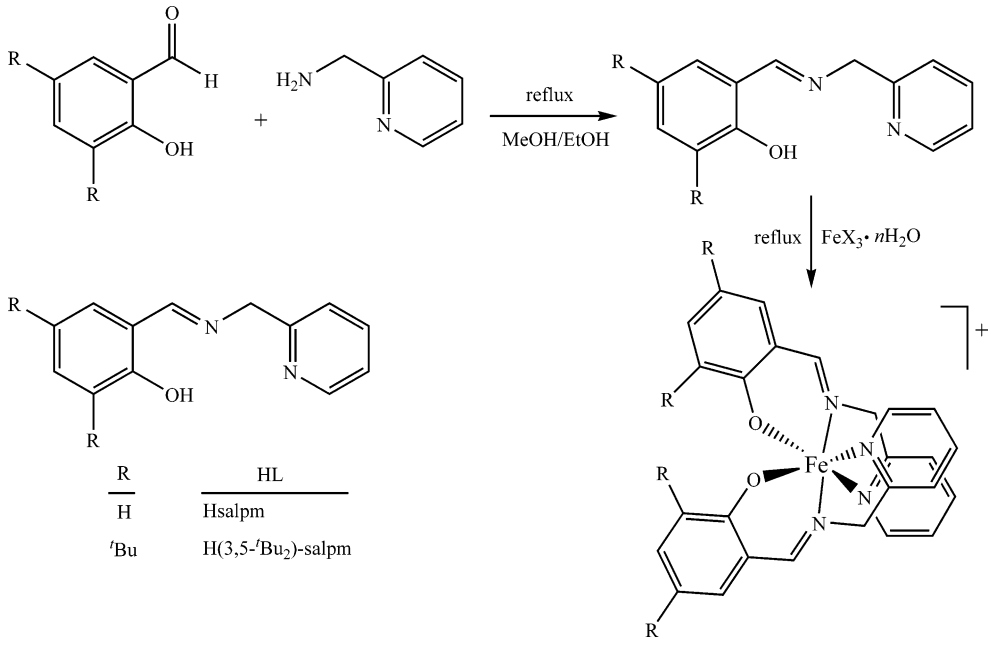

Figure 1. Synthetic route to the mononuclear iron(III) complex cations. Ligand designations: [Hsalpm = *N*-(pyridin-2-ylmethyl)salicylideneamine; H(3,5-^{t}Bu$_2$)-salpm = *N*-(pyridin-2-ylmethyl)-3,5-di-*tert*-butylsalicylideneamine].

complexes with non-heme ferrous enzymes such as soybean lipoxygenase.[23]

In this work, we present mononuclear iron(III) complexes based on two complex cations, viz. $[Fe(salpm)_2]^+$ [Hsalpm = *N*-(pyridin-2-ylmethyl)salicylideneamine (Figure 1)] and $[Fe\{(3,5\text{-}^tBu_2)\text{-salpm}\}_2]^+$ [H(3,5-^{t}Bu$_2$)-salpm = *N*-(pyridin-2-ylmethyl)-3,5-di-*tert*-butylsalicylideneamine (Figure 1)], and we discuss their physicochemical properties mainly in connection with the spin-crossover phenomenon. Variable-temperature crystallographic, magnetic, and spectroscopic (EPR and Mössbauer) data have demonstrated that the iron(III) compound $[Fe(salpm)_2]ClO_4 \cdot 0.5EtOH$ undergoes a thermally induced $^6A_1 \leftrightarrow {}^2T_2$ crossover in the solid state, but the extent of the spin-state conversion is influenced by the sample type. In sharp contrast, the bulky electron-donating *tert*-butyl substituent groups on the ligand framework in the analogous iron(III) complexes $[Fe\{(3,5\text{-}^tBu_2)\text{-salpm}\}_2]NO_3 \cdot 2H_2O$ and $[Fe\{(3,5\text{-}^tBu_2)\text{-salpm}\}_2]X$ (X = ClO_4^- or Cl^-) appear to militate against spin conversion in the solid state; however, in solution, these complexes do undergo spin transformations, though in relatively smaller proportions, as evidenced by EPR spectroscopic measurements around 100 K.

Results and Discussion

Synthetic Strategy and Verification of Formulations. The potentially tridentate mixed-donor Schiff-base ligands *N*-(pyridin-2-ylmethyl)salicylideneamine, Hsalpm, and *N*-(pyridin-2-ylmethyl)-3,5-di-*tert*-butylsalicylideneamine, H(3,5-^{t}Bu$_2$)-salpm, (Figure 1), were synthesized by the condensation reaction of 2-(aminomethyl)pyridine with an equimolar amount of the appropriate aldehyde. The mononuclear iron(III) complexes $[Fe(salpm)_2]ClO_4 \cdot 0.5EtOH$, $[Fe(salpm)_2]Cl$, $[Fe\{(3,5\text{-}^tBu_2)\text{-salpm}\}_2]X$ (X = ClO_4^- or Cl^-) and $[Fe\{(3,5\text{-}^tBu_2)\text{-salpm}\}_2]NO_3 \cdot 2H_2O$ were produced from the reaction of stoichiometric amounts of the respective Schiff-base ligand, generated in situ, with $Fe(ClO_4)_3 \cdot xH_2O$, $FeCl_3 \cdot 6H_2O$ or $Fe(NO_3)_3 \cdot 9H_2O$ in a refluxing mixture of equal volumes of MeOH and EtOH (Figure 1).

Despite the potential danger posed by perchlorate salts as explosives and the problems of the disorder associated with perchlorate counterions in crystallographic studies, the perchlorate ion is useful as a counterion in the crystallization and isolation of transition-metal coordination compounds; however, particular care must be exercised, and only small quantities of the perchlorate salts must be used at a time. In this study, the complexes $[Fe(salpm)_2]ClO_4 \cdot 0.5EtOH$ and $[Fe\{(3,5\text{-}^tBu_2)\text{-salpm}\}_2]ClO_4$ were obtained in crystalline form (in ~80−90% yield) overnight, whereas crystals of the complexes $[Fe(salpm)_2]Cl$, $[Fe\{(3,5\text{-}^tBu_2)\text{-salpm}\}_2]Cl$, and $[Fe\{(3,5\text{-}^tBu_2)\text{-salpm}\}_2]NO_3 \cdot 2H_2O$ were deposited from the solution on slow evaporation over a period of time ranging from 5 days to a fortnight (in ~70−85% yield). Incidentally, the report of Viswanathan et al.[24] on the physical appearance and electronic absorption spectrum of $[Fe(salpm)_2]Cl$ is in conflict with our observations of the physical characteristics of this compound. It was claimed that this compound was dark brown, and a supporting electronic absorption spectrum was provided, which exhibited a weak absorption in the visible region; yet, such iron(III)-phenolate complexes with the chromophore $[FeO_2N_4]$ are well-known for their intense violet-purple colors. Indeed, the black crystals of $[Fe(salpm)_2]Cl$ dissolve readily in MeOH to give an intense purple solution, congruent with the strong LMCT visible absorption.

(23) (a) Galpin, J. R.; Veldink, G. A.; Vliegenthart, J. F. G.; Goldingh, J. *Biochim. Biophys. Acta* **1978**, *536*, 356. (b) Brown, C. A.; Pavlosky, M. A.; Westre, T. E.; Zhang, Y.; Hedman, B.; Hodgson, K. O.; Solomon, E. I. *J. Am. Chem. Soc.* **1995**, *117*, 715.

(24) Viswanathan, R.; Palaniandavar, M.; Balasubramanian, T.; Muthiah, P. T. *J. Chem. Soc., Dalton Trans.* **1996**, 2519.

As expected, the complex $[Fe(salpm)_2]ClO_4 \cdot 0.5EtOH$ behaves likewise in MeOH. The complex $[Fe(salpm)_2]ClO_4$ has been reported previously[25] as an unremarkable member of a series of mononuclear iron(III) complexes, but its X-ray crystal structure and magnetic properties have not been previously studied.

The elemental compositions and chemical formulations of the iron(III) complexes were ascertained by microanalyses − carbon, hydrogen, nitrogen, and chlorine for $[Fe(salpm)_2]ClO_4 \cdot 0.5EtOH$, $[Fe(salpm)_2]Cl$, $[Fe\{(3,5\text{-}{}^tBu_2)\text{-salpm}\}_2]ClO_4$, and $[Fe\{(3,5\text{-}{}^tBu_2)\text{-salpm}\}_2]Cl$, and carbon, hydrogen, and nitrogen for $[Fe\{(3,5\text{-}{}^tBu_2)\text{-salpm}\}_2]NO_3 \cdot 2H_2O$ − and positive-ion fast-atom bombardment (FAB) mass spectrometry. These complexes exhibit similar fragmentation patterns involving two prominent peaks: the higher peak represents the molecular ion and the other the loss of one of the two uninegative ligands, as exemplified by the mass spectra of $[Fe(salpm)_2]ClO_4 \cdot 0.5EtOH$ and $[Fe\{(3,5\text{-}{}^tBu_2)\text{-salpm}\}_2]NO_3 \cdot 2H_2O$. The peak at *m*/*z* 478 represents the parent ion $[Fe(salpm)_2]^+$, whereas the peak at *m*/*z* 267 indicates the dissociation of a salpm ligand from the complex. The mass spectrum of $[Fe(salpm)_2]Cl$ is indistinguishable from that of $[Fe(salpm)_2]ClO_4 \cdot 0.5EtOH$. Similarly, the positive-ion FAB mass spectra of $[Fe\{(3,5\text{-}{}^tBu_2)\text{-salpm}\}_2]ClO_4$, $[Fe\{(3,5\text{-}{}^tBu_2)\text{-salpm}\}_2]Cl$, and $[Fe\{(3,5\text{-}{}^tBu_2)\text{-salpm}\}_2]NO_3 \cdot 2H_2O$ are identical, with the peaks corresponding to $[Fe\{(3,5\text{-}{}^tBu_2)\text{-salpm}\}_2]^+$ and $[Fe(3,5\text{-}{}^tBu_2)\text{-salpm}]^+$ occurring at *m*/*z* 702 and 379, respectively.

Infrared Spectroscopy. Stretching frequencies for selected prominent structural moieties of the Schiff-base ligands and counterions of the iron(III) compounds are compiled in Table S1 in the Supporting Information. The $[Fe(salpm)_2]^+$ and $[Fe\{(3,5\text{-}{}^tBu_2)\text{-salpm}\}_2]^+$ complex cations are readily distinguishable by the characteristic vibrational absorptions of the *tert*-butyl substituent groups of the latter in the range of 2866−2960 cm^{-1}. Although the Schiff bases were not isolated, their formation in situ has been inferred not only from the typical color of these ligands but also from the strong imine absorptions, $\nu_{C=N} = 1610-1618$ cm^{-1}. The IR spectra of all of the complexes were dominated by the vibrations of the phenolate and pyridyl aromatic rings as evidenced by the absorptions ranging from 1415 to 1572 cm^{-1}. The counterions ClO_4^- and NO_3^- are conspicuous by their strong absorption bands and typical wavenumbers: 625 and 1052−1112 cm^{-1} for the former and 1386 cm^{-1} for the latter.

Single-Crystal X-ray Structure Determinations. The intense purplish solutions of $[Fe(salpm)_2]ClO_4 \cdot 0.5EtOH$ and $[Fe\{(3,5\text{-}{}^tBu_2)\text{-salpm}\}_2]NO_3 \cdot 2H_2O$ in MeOH/EtOH (50/50, v/v) deposited black rectangular and diamond-shaped blocks of X-ray-quality crystals in 1 day and 1 week, respectively. For $[Fe(salpm)_2]ClO_4 \cdot 0.5EtOH$, data collection was performed on the same crystal at room temperature, 150 and 100 K, but for $[Fe\{(3,5\text{-}{}^tBu_2)\text{-salpm}\}_2]NO_3 \cdot 2H_2O$, intensity data were recorded only at 150 K. Selected bond distances and angles are compiled in Table 1. A summary of the crystallographic details of the X-ray analyses of these two iron(III) compounds is given in Table 2. The room-temperature X-ray crystal structure of $[Fe\{(3,5\text{-}{}^tBu_2)\text{-salpm}\}_2]ClO_4$ has been reported by Imbert et al.[25] during the preparation of the publication of this work.

The crystal structure of $[Fe(salpm)_2]ClO_4 \cdot 0.5EtOH$, determined at 294, 150, and 100 K, is represented by the ORTEP diagrams in Figure 2 for the X-ray data collected at the lowest of these temperatures. The X-ray structure of $[Fe\{(3,5\text{-}{}^tBu_2)\text{-salpm}\}_2]NO_3 \cdot 2H_2O$ is depicted in Figure 3.

At all three temperatures (294, 150, and 100 K), in the structure of $[Fe(salpm)_2]ClO_4 \cdot 0.5EtOH$, there exist two crystallographically independent mononuclear iron(III) complex cations in the asymmetric unit. Each iron(III) center is pseudo-octahedral with the two mixed-donor tridentate Schiff-base ligands positioned nearly perpendicular to each other and the donor atoms (a phenolate oxygen, an imine nitrogen, and a pyridyl nitrogen) coordinating meridionally in a trans,cis,cis mode. As is usually the case with related transition-metal Schiff-base complexes, the imine nitrogens occupy trans positions.

According to MO theory, the HOMO of HS ($S = {}^5/_2$) octahedral complexes of iron(III) is d_σ*, whereas the HOMO of the corresponding LS ($S = {}^1/_2$) state is d_π (nonbonding). Without exception, the occupancy of the antibonding orbitals in the HS case weakens and, consequently, lengthens the bonds in the coordination sphere. Because Fe−L (L = ligand donor atom) bond distances differ considerably between HS and LS complexes, the average bond distances can be directly correlated with the actual spin state of each iron(III) ion. Single-crystal X-ray crystallography has been employed extensively in this regard to identify spin states of transition-metal complexes.[2e,9d,10a,13,14b,15b,26]

The unit-cell volume of 5363.8(8) $Å^3$ for $[Fe(salpm)_2]ClO_4 \cdot 0.5EtOH$ at 294 K decreases to 5193.3(9) $Å^3$ at 150 K (3.2% reduction) and to 5173.1(9) $Å^3$ at 100 K (3.6% reduction), consistent with the spin-crossover phenomenon.[2e,9d,10a,13,14b,15b,26] The spin crossover in the solid state is a cooperative phenomenon, and the elastic interaction between the spin crossover sites within the crystal lattice is a major factor governing the cooperativity. The packing diagram for $[Fe(salpm)_2]ClO_4 \cdot 0.5EtOH$ (100 K; Figure 1S of the Supporting Information) displays two iron(III) sites arranged in alternating chains.

The average $Fe^{III}-L$ bond distances [complex cation 1: $Fe^{III}-O_{phenolate}$: 1.914(3), $Fe^{III}-N_{imine}$: 2.092(3), and $Fe^{III}-N_{pyridyl}$: 2.169(3) Å; complex cation 2: $Fe^{III}-O_{phenolate}$: 1.907(3), $Fe^{III}-N_{imine}$: 2.105(3), and $Fe^{III}-N_{pyridyl}$: 2.161(3) Å] show that both complex cations in the structure at 294 K are purely high spin ($S = {}^5/_2$). Normal $Fe^{III}-O_{phenolate}$, $Fe^{III}-N_{imine}$, and $Fe^{III}-N_{pyridyl}$ bond distances in related six-

(25) Imbert, C.; Hratchian, H. P.; Lanznaster, M.; Heeg, M. J.; Hryhorczuk, L. M.; McGarvey, B. R.; Schlegel, H. B.; Verani, C. L. *Inorg. Chem.* **2005**, *44*, 7414.

(26) (a) Thompson, A. L.; Goeta, A. E.; Real, J. A.; Galet, A.; Muñoz, M. C. *Chem. Commun.* **2004**, 1390. (b) Matouzenko, G. S.; Bousseksou, A.; Borshch, S. A.; Perrin, M.; Zein, S.; Salmon, L.; Molnar, G.; Lecocq, S. *Inorg. Chem.* **2004**, *43*, 227. (c) Pillet, S.; Hubsch, J.; Lecomte, C. *Eur. Phys. J. B* **2004**, *38*, 541. (d) Yamada, M.; Ooidemizu, M.; Ikuta, Y.; Osa, S.; Matsumoto, N.; Iijima, S.; Kojima, M.; Dahan, F.; Tuchagues, J.-P. *Inorg. Chem.* **2003**, *42*, 8406.

Table 1. Selected Bond Distances (Angstroms) and Angles (Degrees) for $[Fe(salpm)_2]ClO_4$ and $[Fe(3,5\text{-}^tBu_2\text{-salpm})_2]NO_3$

$[Fe(salpm)_2]ClO_4$				$[Fe(3,5\text{-}^tBu_2\text{-salpm})_2]NO_3$	
	294 K	150 K	100 K		150 K
Fe(1)−O(1)	1.917(3)	1.929(2)	1.928(2)	Fe(1)−O(1)	1.894(3)
Fe(1)−O(2)	1.911(3)	1.915(2)	1.914(2)	Fe(1)−O(2)	1.894(3)
Fe(1)−N(1)	2.092(3)	2.089(3)	2.087(2)	Fe(1)−N(2)	2.088(3)
Fe(1)−N(3)	2.093(3)	2.104(2)	2.101(2)	Fe(1)−N(4)	2.080(3)
Fe(1)−N(2)	2.156(4)	2.158(3)	2.160(3)	Fe(1)−N(1)	2.179(3)
Fe(1)−N(4)	2.181(3)	2.174(3)	2.171(2)	Fe(1)−N(3)	2.206(3)
C(1)−O(1)	1.300(5)	1.314(4)	1.320(4)	C(13)−O(1)	1.321(4)
C(14)−O(2)	1.325(5)	1.327(4)	1.319(4)	C(34)−O(2)	1.311(4)
C(7)−N(1)	1.277(6)	1.292(4)	1.298(4)	C(7)−N(2)	1.288(4)
C(8)−N(1)	1.463(4)	1.462(4)	1.472(4)	C(6)−N(2)	1.456(5)
C(20)−N(3)	1.279(5)	1.283(4)	1.282(4)	C(28)−N(4)	1.280(5)
C(21)−N(3)	1.469(5)	1.468(4)	1.478(4)	C(27)−N(4)	1.467(4)
N(1)−Fe(1)−N(3)	168.74(14)	169.33(11)	169.84(10)	N(2)−Fe(1)−N(4)	165.98(13)
O(1)−Fe(1)−N(2)	162.76(13)	163.30(10)	163.35(9)	O(1)−Fe(1)−N(1)	163.09(12)
O(2)−Fe(1)−N(4)	162.85(12)	163.34(9)	163.46(9)	O(2)−Fe(1)−N(3)	160.09(11)
O(1)−Fe(1)−O(2)	94.70(14)	94.51(10)	94.49(9)	O(1)−Fe(1)−O(2)	98.78(11)
O(2)−Fe(1)−N(1)	102.15(12)	101.25(9)	100.75(9)	O(2)−Fe(1)−N(1)	90.34(12)
O(2)−Fe(1)−N(2)	93.93(14)	94.78(10)	94.90(9)	O(2)−Fe(1)−N(2)	105.44(11)
O(2)−Fe(1)−N(3)	86.85(12)	86.97(9)	86.85(9)	O(2)−Fe(1)−N(4)	86.92(12)
O(1)−Fe(1)−N(1)	87.44(13)	88.20(10)	88.39(10)	O(1)−Fe(1)−N(2)	86.96(12)
O(1)−Fe(1)−N(3)	98.66(13)	98.01(10)	97.81(9)	O(1)−Fe(1)−N(3)	93.44(11)
O(1)−Fe(1)−N(4)	89.14(13)	87.55(10)	87.39(9)	O(1)−Fe(1)−N(4)	97.84(12)
N(1)−Fe(1)−N(2)	76.16(15)	76.40(11)	76.37(10)	N(1)−Fe(1)−N(2)	76.85(13)
N(1)−Fe(1)−N(4)	94.70(13)	95.33(10)	95.73(9)	N(1)−Fe(1)−N(3)	82.06(12)
N(2)−Fe(1)−N(3)	96.68(14)	96.31(10)	96.41(10)	N(1)−Fe(1)−N(4)	96.84(12)
N(2)−Fe(1)−N(4)	86.98(13)	87.52(10)	87.51(9)	N(2)−Fe(1)−N(3)	90.79(12)
N(3)−Fe(1)−N(4)	76.04(12)	76.37(10)	76.61(9)	N(3)−Fe(1)−N(4)	75.82(12)
Fe(1)−O(1)−C(1)	134.0(3)	133.1(2)	132.5(2)	Fe(1)−O(1)−C(13)	136.3(3)
Fe(1)−O(2)−C(14)	130.9(2)	130.31(19)	130.44(19)	Fe(1)−O(2)−C(34)	135.2(2)
Fe(2)−O(3)	1.896(3)	1.850(3)	1.857(2)		
Fe(2)−O(4)	1.917(3)	1.882(2)	1.881(2)		
Fe(2)−N(5)	2.106(3)	1.971(3)	1.951(3)		
Fe(2)−N(7)	2.103(3)	1.981(3)	1.954(2)		
Fe(2)−N(6)	2.166(3)	2.039(3)	2.010(2)		
Fe(2)−N(8)	2.156(3)	2.030(3)	2.002(2)		
C(27)−O(3)	1.311(5)	1.316(5)	1.321(4)		
C(40)−O(4)	1.315(4)	1.333(4)	1.328(4)		
C(33)−N(5)	1.271(5)	1.292(4)	1.287(4)		
C(34)−N(5)	1.465(5)	1.464(4)	1.467(4)		
C(46)−N(7)	1.289(5)	1.286(4)	1.287(4)		
C(47)−N(7)	1.463(5)	1.466(4)	1.470(4)		
N(5)−Fe(2)−N(7)	169.02(13)	175.42(11)	177.36(10)		
O(3)−Fe(2)−N(6)	163.63(13)	172.74(11)	174.47(10)		
O(4)−Fe(2)−N(8)	161.55(13)	170.24(10)	172.13(10)		
O(3)−Fe(2)−O(4)	96.31(14)	95.32(11)	94.96(10)		
O(4)−Fe(2)−N(5)	101.21(12)	91.57(10)	89.31(10)		
O(4)−Fe(2)−N(6)	88.74(12)	88.48(9)	88.62(9)		
O(4)−Fe(2)−N(7)	87.30(12)	92.17(10)	93.06(10)		
O(3)−Fe(2)−N(5)	87.29(13)	93.03(12)	93.97(11)		
O(3)−Fe(2)−N(7)	98.76(13)	89.26(12)	87.00(11)		
O(3)−Fe(2)−N(8)	94.00(14)	90.86(12)	90.44(10)		
N(5)−Fe(2)−N(6)	76.44(13)	80.65(11)	81.84(10)		
N(5)−Fe(2)−N(8)	94.51(13)	95.65(11)	96.03(10)		
N(6)−Fe(2)−N(7)	97.01(13)	96.80(10)	97.04(10)		
N(6)−Fe(2)−N(8)	85.60(13)	86.23(10)	86.44(10)		
N(7)−Fe(2)−N(8)	76.02(13)	80.34(10)	81.50(10)		
Fe(2)−O(3)−C(27)	135.2(3)	129.3(3)	127.4(2)		
Fe(2)−O(4)−C(40)	132.3(2)	127.42(19)	126.42(19)		

coordinate high-spin complexes are in the ranges 1.895−1.938,[4b,12d,27] 2.051−2.155,[4b,12c,d,27a] and 2.168−2.224 Å,[24,27a] respectively, whereas the corresponding distances in the LS state tend to be in the ranges 1.850−1.885,[12c,14b] 1.905−1.961,[12c,14b] and 1.993−2.024 Å,[28] respectively.

In the structure of $[Fe(salpm)_2]ClO_4 \cdot 0.5EtOH$ at 100 K, one of the two complex cations is in the HS state and the other is in the LS state. The bond distances of the HS complex cation are crystallographically indistinguishable from those of the two HS complex cations at 294 K (Table 1). The difference between the overall averages of the HS and LS Fe−L bond distances for the two cations at 100 K, $\Delta R([FeO_2N_4])$, is 0.12 Å [with the largest difference occurring in the most compressible $Fe-N_{pyridyl}$ bonds, $\Delta R(Fe-N) = 0.16$ Å, and the smallest in the strongest $Fe-O_{phenolate}$ bonds, $\Delta R(Fe-O) = 0.05$ Å]. Previously, a correlation between Fe−L bond distances and spin states (HS and LS)

(27) (a) Lubben, M.; Meetsma, A.; van Bolhus, F.; Feringa, B. L.; Hage, R. *Inorg. Chim. Acta* **1994**, *215*, 123. (b) Hamalainen, R.; Turpeinen, U. *Acta Chem. Scand.* **1989**, *43*, 15.

(28) Arulsamy, N.; Hodgson, D. J. *Inorg. Chem.* **1994**, *33*, 4531.

Table 2. Selected Crystallographic Data for $[Fe(salpm)_2]ClO_4$ and $[Fe\{(3,5\text{-}^tBu_2)\text{-}salpm\}_2]NO_3\cdot 2H_2O$

	$[Fe(salpm)_2]ClO_4$			$[Fe\{(3,5\text{-}^tBu_2)\text{-}salpm\}_2]NO_3\cdot 2H_2O$
	294 K	150 K	100 K	150 K
empirical formula	$C_{26}H_{22}ClFeN_4O_6$	$C_{26}H_{22}ClFeN_4O_6$	$C_{26}H_{22}ClFeN_4O_6$	$C_{42}H_{58}FeN_5O_7$
fw	577.78	577.78	577.78	800.78
cryst syst	monoclinic	monoclinic	monoclinic	triclinic
space group	$P2_1/n$	$P2_1/n$	$P2_1/n$	$P\bar{1}$
a (Å)	15.8851(13)	15.4403(16)	15.3694(16)	10.910(3)
b (Å)	19.4045(16)	19.300(2)	19.292(2)	11.720(3)
c (Å)	17.4238(14)	17.4482(17)	17.4788(17)	17.851(4)
α (deg)	90	90	90	102.968(4)
β (deg)	92.915(2)	92.772(2)	92.869(2)	90.510(5)
γ (deg)	90	90	90	108.318(5)
V (Å^3)	5363.8(8)	5193.3(9)	5173.1(9)	2103.8(8)
Z	8	8	8	2
ρ_{calcd} (Mg/m^3)	1.431	1.478	1.483	1.264
μ (mm^{-1})	0.709	0.732	0.735	0.412
collected reflns	23 915	23 060	22 824	11 216
independent reflns	7753	7538	7449	6051
R_{int}	0.0437	0.0500	0.0501	0.0510
R [$I > 2\sigma(I)$]	0.0462	0.0400	0.0375	0.0532
wR (all data)	0.1445	0.0939	0.0942	0.1168

in pseudo-octahedral iron(III) complexes indicated that the difference between the overall averages, $\Delta R([FeO_2N_4])$, of the Fe−L bond distances in the pure forms of the HS and LS states lies in the range 0.12−0.15 Å.[4b,13,15b] Hence, in $[Fe(salpm)_2]ClO_4\cdot 0.5EtOH$, one metal center is purely HS, whereas the other is purely LS at 100 K, implying that one of the complex cations has undergone a complete spin transition ($S = {}^5/_2 \rightarrow S = {}^1/_2$), whereas the other has retained the HS state down to 100 K.

Despite the growing interest in the use of variable-temperature X-ray analysis to monitor spin-transitions in spin-crossover systems, observation of crystallographically independent pure HS and LS metal centers for a given mononuclear iron(III) complex at the same temperature remains an extremely rare occurrence. Commonly, in cases where two crystallographically distinct molecules coexist, two scenarios are possible: (1) both metal centers are HS or LS (e.g., both HS in $[Fe(saltrien)]PF_6$[12d] and $[Fe(pap)_2]ClO_4\cdot H_2O$[10b] at room temperature, and both LS in $[Fe(pap)_2]PF_6\cdot MeOH$[10c] at 90 K and $[Fe(3\text{-}OEt\text{-}SalAPA)_2]ClO_4\cdot C_6H_6$[14b] at 128 K); (2) the spin state at each metal center is impure (e.g., ∼20% HS at one metal center and ∼60% HS at the other in $[Fe(3\text{-}OEt\text{-}SalAPA)_2]ClO_4\cdot C_6H_5Br$[14b] at 163 K). Recently, Que et al. reported the crystal structure of $[(N4Py)Fe(OMe)](ClO_4)_2$,[19] which consists of two distinct complex cations in the asymmetric unit: one is purely HS, whereas the other exhibits bond distances intermediate between those typically observed in LS iron(III) and HS iron(III) complexes, consistent with the spin-transition curve obtained from magnetic susceptibility measurements.

Conspicuously, the compression of the Fe−L bonds in $[Fe(salpm)_2]ClO_4\cdot 0.5EtOH$ emanating from the HS → LS conversion is accompanied by a structural modification of the overall coordination sphere. The geometry at the metal center becomes noticeably more regular despite the ligand constraints imposed by the relatively rigid hetero-donor coordination environment. Notably, on cooling the compound from room temperature to 100 K, there is a steady increase in the axial $N_{imine}-Fe-N_{imine}$ and the equatorial $O_{phenolate}-Fe-N_{pyridyl}$ angles toward linearity (Table 1). To effect this structural change at the $[FeO_2N_4]$ core, the two phenolate Fe−O−C angles have had to decrease from 135 to 127° [Fe(2)−O(3)−C(27)] and from 132 to 126° [Fe(2)−O(4)−C(40)], approaching the idealized sp^2-hybridization angle,[29] as a consequence of increasing delocalization of the phenolate negative charge over the aromatic ring. The phenolate Fe−O−C angle is sometimes used as a gauge of the extent of the distortion of the geometry at the metal center, often arising from steric effects.[30] On the whole, the ligand framework was unaffected by the spin crossover; the characteristic Schiff-base C═N bond distances remained virtually the same (Table 1).

The overall structure of the complex cation $[Fe\{(3,5\text{-}^tBu_2)\text{-}salpm\}_2]^+$ determined at 150 K (Figure 3) resembles that of $[Fe(salpm)_2]^+$ in terms of the coordination arrangement of the donor atoms (a phenolate oxygen, an imine nitrogen, and a pyridyl nitrogen) and the orientation of the tridentate Schiff-base ligands. The geometry at the metal center is best described as distorted octahedral. The Fe−L bond distances in the room-temperature structure of $[Fe\{(3,5\text{-}^tBu_2)\text{-}salpm\}_2]ClO_4$ [monoclinic, space group $P2(1)/c$][25] are comparable with those in the low-temperature structure of $[Fe\{(3,5\text{-}^tBu_2)\text{-}salpm\}_2]NO_3\cdot 2H_2O$ (Table 1) and are consistent with the high-spin state of the iron(III) ion. Thus, the adverse effect of the bulky *tert*-butyl substituent groups on the spin-crossover phenomenon in the solid state is evident. The degree of electronic and steric influence of substituent groups on spin crossovers has been demonstrated previously.[13,15b] Structurally, the steric effect of the *tert*-butyl groups is manifested in the phenolate Fe−O−C angles: 137.5 and 136.4° for $[Fe\{(3,5\text{-}^tBu_2)\text{-}salpm\}_2]ClO_4$ (at 295 K);[25] 136.3 and 135.2° for $[Fe\{(3,5\text{-}^tBu_2)\text{-}salpm\}_2]NO_3\cdot 2H_2O$ (at 150 K). The extent of the distortion of the geometry at the metal center, resulting from the overall ligand constraints, can be

(29) (a) Viswanathan, R.; Palaniandavar, M.; Balasubramanian, T.; Muthiah, T. P. *Inorg. Chem.* **1998**, *37*, 2943. (b) Velusamy, M.; Palaniandavar, M.; Gopolan, R. S.; Kulkarni, G. U. *Inorg. Chem.* **2003**, *42*, 8283.
(30) Velusamy, M.; Mayilmurugan, R.; Palaniandavar, M. *Inorg. Chem.* **2004**, *43*, 6284.

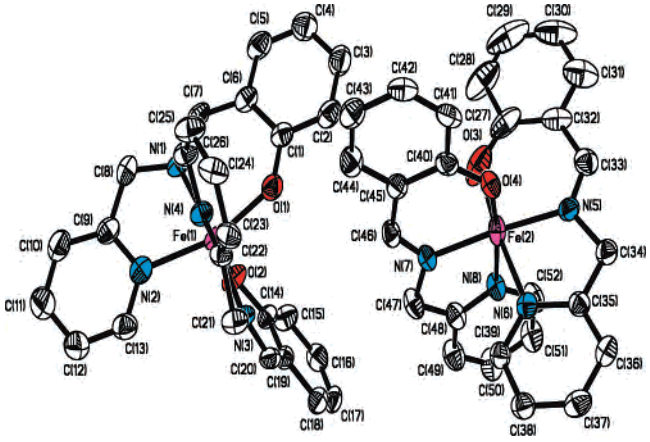

Figure 2. View of the two independent complex cations in the X-ray crystal structure of $[Fe(salpm)_2]ClO_4 \cdot 0.5EtOH$ at 100 K.

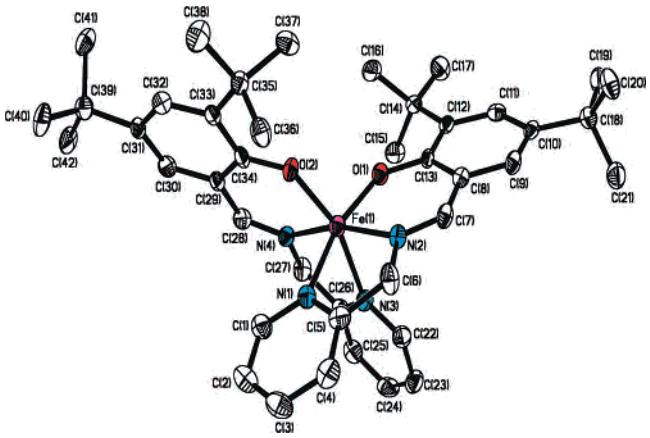

Figure 3. View of the complex cation in the X-ray crystal structure of $[Fe\{(3,5\text{-}^tBu_2)\text{-salpm}\}_2]NO_3 \cdot 2H_2O$ at 150 K.

judged by the considerable deviations from idealized angles for O_h symmetry.

Magnetism. Spin-crossover behavior is best analyzed using variable-temperature magnetic susceptibility measurements. For normal paramagnetism of mononuclear octahedral iron(III) complexes, the effective magnetic moments (μ_{eff}) range from ~2.0 μ_B ($\chi_M T$ = ~0.50 cm^3 mol^{-1} K) to ~6.0 μ_B ($\chi_M T$ = ~4.5 cm^3 mol^{-1} K): ~2.0−2.6 μ_B (LS iron(III)) and ~5.5−6.0 μ_B (HS iron(III)). The orbital contribution to the LS magnetic moments is considerable at or around room temperature.[28] At 4 K, the LS magnetic moments of the vast majority of octahedral iron(III) complexes are around 2 μ_B when the spin transition is complete.[4,9d,10b,c,12a,14b,15a] Figure 4 shows two spin-transition curves obtained from plots of μ_{eff} versus T for two samples of $[Fe(salpm)_2]ClO_4 \cdot 0.5EtOH$, one crystalline and the other a powder. In the crystalline form [5.90 μ_B (300 K) ≥ μ_{eff} ≥ 2.65 μ_B (65 K)], the spin crossover $^6A_{1g}$ ($S = {}^5/_2$) ↔ $^2T_{2g}$ ($S = {}^1/_2$) occurs in two steps [$T_{c(S1)}$ = ~180 K and $T_{c(S2)}$ = ~100 K]; between 65 and 5 K, the value of μ_{eff} is constant and represents approximately 10% residual HS state.

The spin-transition curve for the powder sample also demonstrates a two-step spin-crossover [$T_{c(S1)}$ = ~180 K and $T_{c(S2)}$ = ~95 K] as shown by magnetic susceptibility measurements (Figure 4), but, interestingly, the curve levels off at μ_{eff} = 4.13 μ_B (70 K) [cf. μ_{eff} = 2.65 μ_B (~65 K) in the crystalline sample]. This behavior exemplifies the adverse effect of sample grinding on spin crossovers. Although it has been demonstrated previously that grinding a sample causes the spin transition to be more gradual and incomplete,[7,14b,15] the magnitude of this effect has never been greater than that observed in the present system. This study highlights the importance of sample handling in spin-crossover systems.

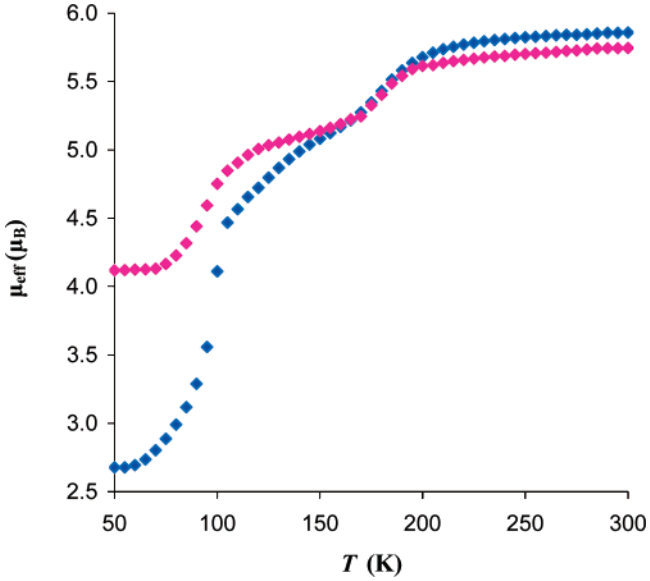

Figure 4. Variation of the magnetic moments of $[Fe(salpm)_2]ClO_4 \cdot 0.5EtOH$ with temperature (blue for the crystals and purple for the powder).

The room-temperature effective magnetic moments [$(8\chi_M T)^{1/2}$] of the complexes $[Fe\{(3,5\text{-}^tBu_2)\text{-salpm}\}_2]Cl$, $[Fe\{(3,5\text{-}^tBu_2)\text{-salpm}\}_2]ClO_4$, and $[Fe\{(3,5\text{-}^tBu_2)\text{-salpm}\}_2]NO_3 \cdot 2H_2O$ are 5.85, 5.90, and 5.89 μ_B, respectively, pointing to the existence of the iron(III) in the high-spin state, $[4S(S+1)]^{1/2}$ = 5.92 μ_B. This spin state is retained down to 5 K in the solid state.

Mössbauer Spectroscopy. The magnetic behavior of $[Fe(salpm)_2]ClO_4 \cdot 0.5EtOH$ is supported by Mössbauer spectroscopy.[4a,10b,12a,14b,15a] Figure 5 shows a variable-temperature Mössbauer study of the spin transition in $[Fe(salpm)_2]ClO_4 \cdot 0.5EtOH$. At 300 K, the Mössbauer spectrum displays a doublet consistent with the HS state of $[Fe(salpm)_2]ClO_4 \cdot 0.5EtOH$ ($S = {}^5/_2$, ΔE_Q = 0.71 mm s^{-1}, δ = 0.39 mm s^{-1}). Around 200 K, a new outer doublet associated with the LS state emerges and intensifies on further cooling, at the expense of the HS doublet. At 70 and 15 K, the Mössbauer spectra are virtually identical with the intensity of the outer (LS) doublet ($S = {}^1/_2$, ΔE_Q = 2.68 mm s^{-1}, δ = 0.19 mm s^{-1}), pointing to ~90% of the complex cations existing in the LS state (i.e., ~10% HS remnant). Mössbauer spectroscopy confirmed the magnetic data that T_c = ~ 100 K and revealed that at this temperature, half of the complex cations are HS and the other half are LS. Hence, at 100 K the crystalline sample of $[Fe(salpm)_2]ClO_4 \cdot 0.5EtOH$ is expected to exhibit a magnetic moment around 4 μ_B,[19] and indeed it does, μ_{eff} = 4.11 μ_B. Taking into account the crystallographic, magnetic, and Mössbauer spectroscopic data, it can be inferred that, in the crystalline form, $[Fe(salpm)_2]ClO_4 \cdot 0.5EtOH$ undergoes a very nearly complete

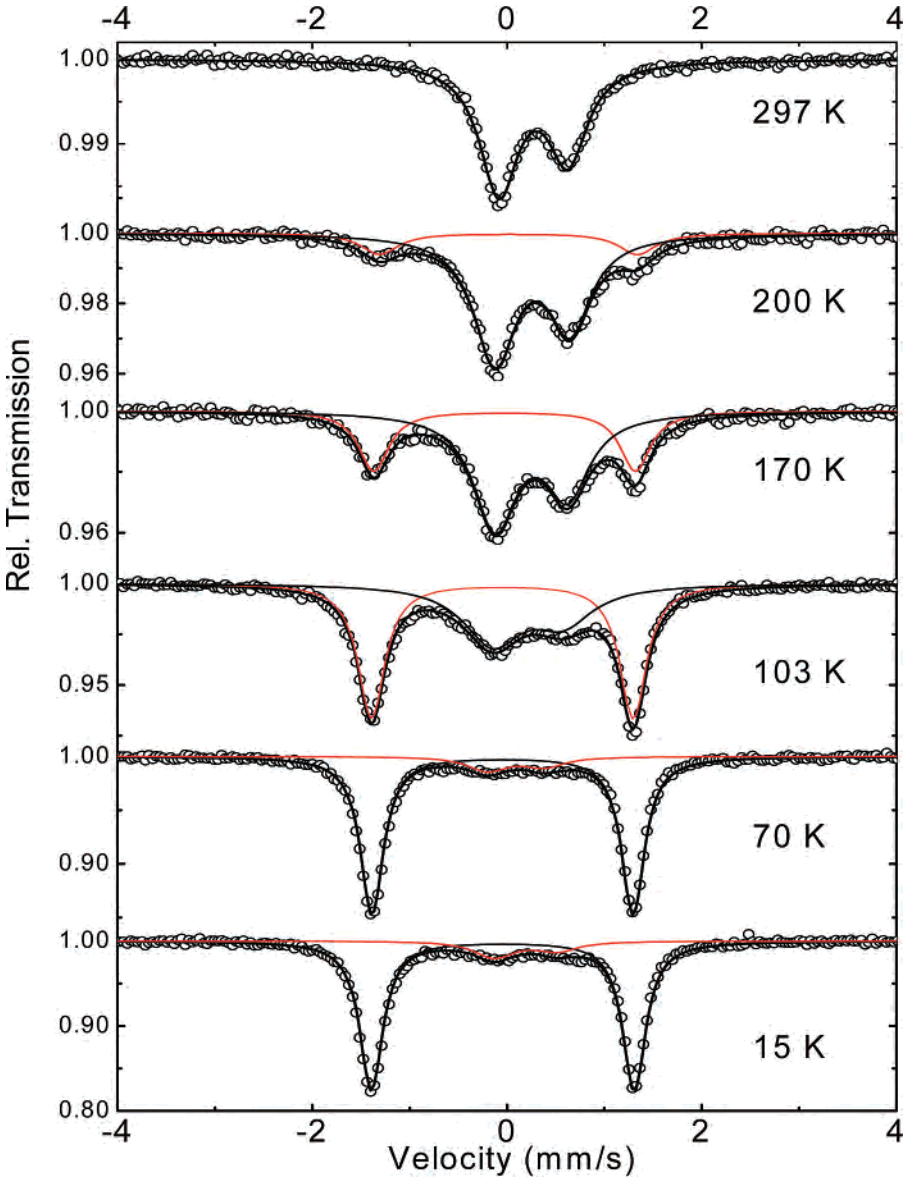

Figure 5. Mössbauer spectra of $[Fe(salpm)_2]ClO_4 \cdot 0.5EtOH$.

two-step, two-site, spin-crossover over the temperature range 300−5 K. At room temperature, both complex cations are in the HS state. On cooling to 100 K, one of the complex cations completely converts to LS, whereas the other remains in the HS state. The spin transformation of the second complex cation occurs in the temperature range 100−70 K but never reaches completion (with ∼10% HS remnant); below 70 K, the magnetic data and Mössbauer spectra are independent of temperature.

EPR Spectroscopy. The high-spin nature of the complexes $[Fe\{(3,5\text{-}^tBu_2)\text{-salpm}\}_2]Cl$, $[Fe\{(3,5\text{-}^tBu_2)\text{-salpm}\}_2]ClO_4$, and $[Fe\{(3,5\text{-}^tBu_2)\text{-salpm}\}_2]NO_3 \cdot 2H_2O$ has been corroborated by solid-state EPR spectroscopy, as exemplified by the room-temperature X-band EPR powder spectrum of $[Fe\{(3,5\text{-}^tBu_2)\text{-salpm}\}_2]Cl$, which exhibits a strong resonance at $g = 4.17$ and a weaker one at $g = 9.40$ (Figure 6a), a characteristic feature for rhombically distorted octahedral iron(III) complexes with the $^6A_1$ electronic ground state.[12a,b,14b,15b,31] This spectrum remains unchanged down to 100 K, save a slight broadening of the weaker resonance. Indeed, as observed in the X-ray crystal structures of $[Fe\{(3,5\text{-}^tBu_2)\text{-salpm}\}_2]ClO_4$[25] at room temperature and $[Fe\{(3,5\text{-}^tBu_2)\text{-salpm}\}_2]NO_3 \cdot 2H_2O$ at 150 K as well as the magnetic measurements, these iron(III) complexes, bearing bulky groups on the phenolate moiety, favor the high-spin state in the solid state. However, in solution, spin conversion does occur, though modestly, as illustrated by the EPR spectrum of $[Fe\{(3,5\text{-}^tBu_2)\text{-salpm}\}_2]Cl$ in MeOH at 100 K (Figure 6b). At this low temperature, the complex is still predominantly in the high-spin state [$g = \sim 9.10$ (weak) and 4.15 (strong)]; the existence of a small but significant fraction of the $[Fe\{(3,5\text{-}^tBu_2)\text{-salpm}\}_2]^+$ complex ions in the low-spin state is indicated by the weak signal at $g = \sim 2$. This EPR result is consistent with the observation of Imbert et al.[25] for $[Fe\{(3,5\text{-}^tBu_2)\text{-salpm}\}_2]ClO_4$

(31) (a) Shongwe, M. S.; Smith, R.; Marques, H. M.; van Wyk, J. A. *J. Inorg. Biochem.* **2004**, *98*, 199. (b) Shongwe, M. S.; Kaschula, C. H.; Adsetts, M. S.; Ainscough, E. W.; Brodie, A. M.; Morris, M. J. *Inorg. Chem.* **2005**, *44*, 3070.

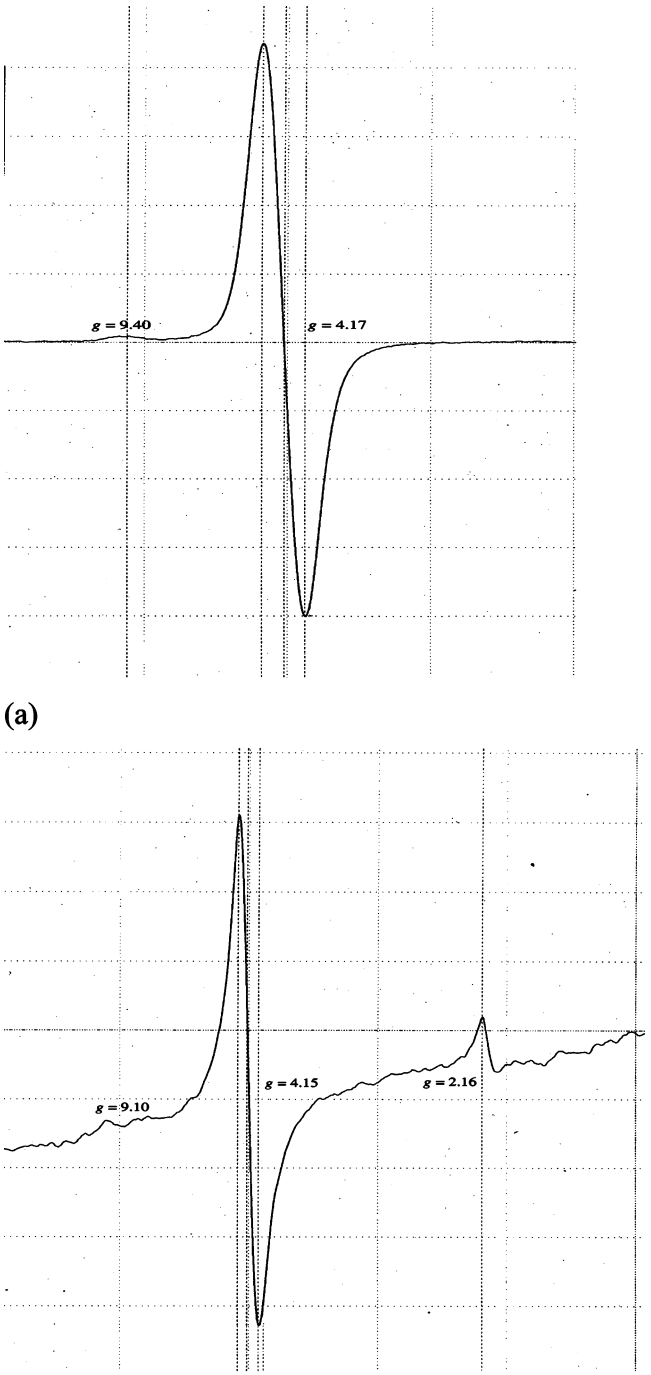

Figure 6. X-band EPR spectra of [Fe{(3,5-^{t}Bu$_2$)-salpm}$_2$]Cl at (a) room temperature (powder) and (b) 100 K (frozen MeOH solution).

in frozen acetone solution at 115 K. Remarkably, as was observed in the solid state using X-ray crystallography, magnetic susceptibility measurements, and Mössbauer spectroscopy, in a frozen methanol solution at 100 K, [Fe(salpm)$_2$]-ClO_4·0.5EtOH undergoes spin conversion that yields approximately equal proportions of the HS and LS complex cations. The resonances at $g = 9.20$ and 4.21 are ascribed to the $S = {}^5/_2$ iron(III) centers, whereas the signals at $g =$ 2.20, 2.16, and 1.94 are associated with the $S = {}^1/_2$ iron(III) centers in this spin-crossover compound (Figure 7).[12a,b,14b,15b,19,31,32]

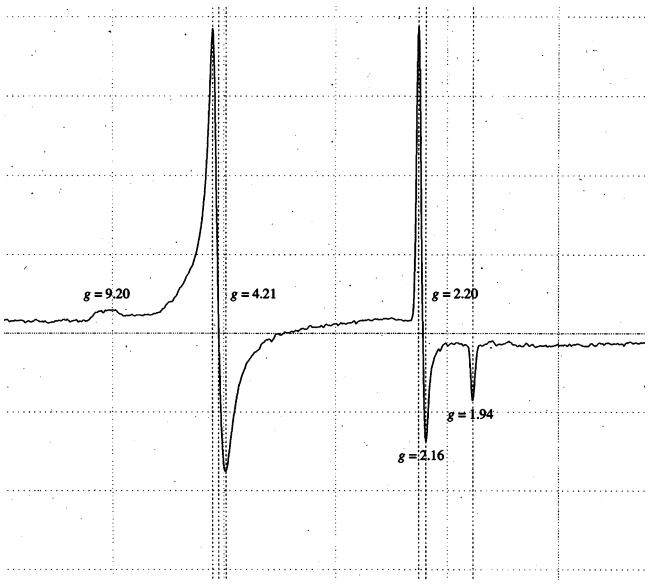

Figure 7. X-band EPR spectrum of [Fe(salpm)$_2$]ClO_4·0.5EtOH at 100 K (frozen MeOH solution).

Electronic Spectroscopy. As already established magnetically, and in some cases crystallographically and spectroscopically, the complexes reported herein have iron(III) centers with a high-spin d^5 configuration at room temperature. As such, ligand-field transitions are expected to be spin-forbidden and the corresponding absorption bands to be obscured by charge-transfer bands. UV−visible spectroscopy shows two LMCT bands as dominant features in the 300−700 nm region of the electronic spectrum. The UV−visible spectra of [Fe(salpm)$_2$]ClO_4·0.5EtOH and Fe{(3,5-^{t}Bu$_2$)-salpm}$_2$]ClO_4 in MeOH are depicted in Figure S2 of the Supporting Information: [Fe(salpm)$_2$]ClO_4·0.5EtOH: λ_{max} = 328 nm (ϵ = 8100 L mol^{-1} cm^{-1}), λ_{max} = 530 nm (ϵ = 2800 L mol^{-1} cm^{-1}); Fe{(3,5-^{t}Bu$_2$)-salpm}$_2$]ClO_4: λ_{max} = 345 nm (ϵ = 10 500 L mol^{-1} cm^{-1}), λ_{max} = 575 nm (ϵ = 3500 L mol^{-1} cm^{-1}). The UV absorption is attributable to a phenolate (p_π) → iron(III) (d_{σ^*}) charge-transfer transition, whereas the visible absorption is consistent with the charge-transfer transition from the phenolate p_π orbital to a half-filled d_{π^*} orbital of the central metal atom.[25,31,33] The latter LMCT absorption is responsible for the intense colors of these complexes. The differences between the energies of the LMCT absorptions for [Fe(salpm)$_2$]ClO_4·0.5EtOH and [Fe{(3,5-^{t}Bu$_2$)-salpm}$_2$]ClO_4 (11 620 and 11 600 cm^{-1}, respectively) are an estimate of Δ_o for these complexes, and these values compare favorably with those reported for related HS iron(III)-phenolate mononuclear complexes.[31b,33a,33c] As expected, the *tert*-butyl groups have very little effect on the ligand-field strength of the Schiff base. However,

(32) (a) Patra, A. K.; Olmstead,M. M.; Mascharak, P. K. *Inorg. Chem.* **2002**, *41*, 5403. (b) Sreerama, S. G.; Mukhopadhyay, A.; Pal, S. *Inorg. Chem. Commun.* **2006**, *9*, 1083. (c) Kannappan, R.; Tanase, S.; Mutikainen, I.; Turpeinen, U.; Reedijk, J. *Polyhedron* **2006**, *25*, 1646. (c) Bautz, J.; Comba, P.; Que, Jr., L. *Inorg. Chem.*, **2006**, *45*, 7077.
(33) (a) Gaber, B. P.; Miskowski, V. P.; Spiro, T. G. *J. Am. Chem. Soc.* **1974**, *96*, 6868. (b) Ainscough, E. W.; Brodie, A. M.; Plowman, J. E.; Brown, K. L.; Addison, A. W.; Gainsford, A. R. *Inorg. Chem.* **1980**, *19*, 3655. (c) Setyawati, I. A.; Rettig, S. J.; Orvig, C. *Can. J. Chem.* **1999**, *77*, 2033.

conspicuously, on substituting the hydrogen atoms at positions 3 and 5 of the phenolate moiety with the electron-donating *tert*-butyl groups, the LMCT bands shift bathochromically. The electronic effect of substituent groups on charge-transfer transitions in phenolate-containing complexes has been demonstrated previously.[25,31b,33b,34,35] Electron-donating groups facilitate LMCT transitions, thereby lowering their energies; the converse is true for electron-withdrawing groups.[33b,34,35]

Concluding Remarks

This report has focused attention on the spin-crossover behavior of the mononuclear ferric compound $[Fe(salpm)_2]ClO_4 \cdot 0.5EtOH$ in the solid state. Crystallographic, magnetic, and spectroscopic data have revealed that this compound undergoes a two-step, two-site, spin transition, which is complete at one of the two crystallographically independent metal centers but incomplete at the other. This spin-crossover system has been shown to be sensitive to temperature and sample grinding. The steric and electronic effects of ring substituent groups on spin-crossovers and electronic structures, respectively, have been explored using the complexes $Fe\{(3,5\text{-}{}^tBu_2)\text{-salpm}\}_2]X$ ($X = ClO_4^-$, NO_3^-, or Cl^-) possessing the bulky and electron-donating *tert*-butyl groups. Interestingly, although these complexes do not exhibit a spin transformation in the solid state, in solution they behave otherwise, though modestly so. The *tert*-butyl groups promote LMCT transitions, and their influence is much more pronounced for the phenolate (p_π) $\rightarrow$ iron(III) (d_{π^*}) charge-transfer transition in the visible region.

Experimental Section

Materials and Physical Techniques. Unless otherwise stated, all of the starting materials were obtained at the highest levels of purity possible from commercial sources and used as received. The solvents MeOH and EtOH were purified and dried by heating for several hours under reflux in the presence of magnesium and iodine and, subsequently, distilling. Infrared spectra of the complexes were recorded on a Nicolet Impact 400D FTIR spectrophotometer in the range 4000−400 cm^{-1} with the samples compressed as KBr disks. Electronic absorption spectra were measured using an HP8453 UV-Visible spectrophotometer in the range 200−1100 nm. Measurements of fast atom bombardment (FAB) mass spectra in the positive mode were performed on a VG 70-SE mass spectrometer, using 3-nitrobenzyl alcohol as matrix. Variable-temperature (4−300 K) magnetic susceptibility measurements were carried out on a Quantum Design MPMS-5S SQUID magnetometer operating at a magnetic field of 0.5 T with $HgCo(NCS)_4$ as the calibrant. Diamagnetic corrections were performed in the usual way using Pascal's constants. Variable-temperature Mössbauer spectra were recorded on a conventional spectrometer equipped with a Janis cryostat, using a Lakeshore temperature controlling device and a calibrated silicon diode thermometer. $^{57}Co(Rh)$ was used as the source of the radiation. First-derivative X-band EPR spectra of powders and frozen solutions (MeOH) of the complexes were obtained at selected temperatures from 298 to 100 K on a JEOL JES-FA200 spectrometer, using liquid nitrogen as the coolant and (diphenylpicryl)hydrazyl (DPPH) as the standard for the calibration of the spectral *g* values.

X-ray Crystal Structure Determinations. Single-crystal X-ray diffraction data collection and analyses were performed on a Bruker SMART 1K CCD area detector diffractometer equipped with Mo Kα radiation ($\lambda = 0.71073$ Å). The crystallographic measurements were carried out at 294, 150, and 100 K for $[Fe(salpm)_2]ClO_4 \cdot 0.5EtOH$ and only at 150 K for $[\{(3,5\text{-}Bu_2)\text{-salpm}\}_2]NO_3 \cdot 2H_2O$. Data processing was carried out using *SMART* and *SHELX* software. In the case of $[Fe(salpm)_2]ClO_4 \cdot 0.5EtOH$, one of the perchlorate counterions exhibited a disorder.

Synthesis of $[Fe(salpm)_2]ClO_4 \cdot 0.5EtOH$. Reaction of salicylaldehyde (0.1221 g, 1.0 mmol) with 2-(aminomethyl)pyridine (0.1081 g, 1.0 mmol) in a refluxing mixture of MeOH/EtOH (30 mL, 1:1 v/v) for 15 min afforded a yellow solution of the ligand *N*-(pyridine-2-ylmethyl)salicylideneamine (Hsalpm). Addition of $Fe(ClO_4)_3 \cdot xH_2O$ (0.1771 g, 0.50 mmol) to this solution resulted in an intense purple solution instantaneously. Upon standing at room temperature overnight, the solution produced black rectangular blocks of crystals (0.2391 g, 79.6% yield). The yield depended on the duration of the crystallization process. Anal. Calcd for $[C_{27}H_{25}ClFeN_4O_{6.5}]$: C, 53.98; H, 4.19; N, 9.33; Cl, 5.90. Found: C, 53.79; H, 4.17; N, 9.42; Cl, 5.95. FAB MS (+ve mode): *m*/*z* 478, 267.

Synthesis of $[Fe(salpm)_2]Cl$. The complex $[Fe(salpm)_2]Cl$ was produced in 82.3% yield following closely the procedure described for the synthesis of $[Fe(salpm)_2]ClO_4 \cdot 0.5EtOH$ but using $FeCl_3 \cdot 6H_2O$ instead of $Fe(ClO_4)_3 \cdot xH_2O$. Needle-like crystals of the complex were obtained on slow evaporation of the solution over a fortnight. Anal. Calcd for $[C_{26}H_{22}ClFeN_4O_2]$: C, 60.78; H, 4.32; N, 10.90; Cl, 6.90. Found: C, 60.72; H, 4.30; N, 10.85; Cl, 6.93. FAB MS (+ve mode): *m*/*z* 478, 267.

Synthesis of $[Fe\{(3,5\text{-}{}^tBu_2)\text{-salpm}\}_2]ClO_4$. 3.5-Di-*tert*-butylsalicylaldehyde (0.2343 g, 1.0 mmol) was dissolved completely in a solvent mixture of MeOH/EtOH (30 mL, 1:1 v/v). On addition of 2-(aminomethyl)pyridine (0.1081 g, 1.0 mmol) to this colorless solution, a strong yellow color developed immediately. This solution was heated under reflux for 15 min, after which $Fe(ClO_4)_3 \cdot xH_2O$ (0.1771 g, 0.50 mmol) was added with swirling, resulting in the instantaneous formation of an intense purplish indigo solution. Within 6 h of standing at room temperature, the solution deposited black diamond-shaped blocks of crystals; however, the process of crystallization was allowed to continue overnight to maximize the yield. Yield: 0.3600 g (89.8%). Anal. Calcd for $[C_{42}H_{54}ClFeN_4O_6]$: C, 62.88; H, 6.78; N, 6.98; Cl, 4.42. Found: C, 62.79; H, 6.76; N, 6.88; Cl, 4.40. FAB MS (+ve mode): *m*/*z* 702, 379.

Synthesis of $[Fe\{(3,5\text{-}{}^tBu_2)\text{-salpm}\}_2]Cl$. The complex $[\{Fe(3,5\text{-}{}^tBu_2)\text{-salpm}\}_2]Cl$ was produced from the reaction of 3.5-di-*tert*-butylsalicylaldehyde (0.2343 g, 1.0 mmol), 2-(aminomethyl)pyridine (0.1081 g, 1.0 mmol), and $FeCl_3 \cdot 6H_2O$ (0.1352 g, 0.50 mmol), following a procedure analogous to that described for the synthesis of $[\{Fe(3,5\text{-}{}^tBu_2)\text{-salpm}\}_2]ClO_4$. The complex was obtained as black rectangular blocks from the purplish indigo solution on slow evaporation at room temperature over a period of approximately 2 weeks. Yield: 0.3156 g (85.5%). Anal. Calcd for $[C_{42}H_{54}ClFeN_4O_2]$: C, 68.34; H, 7.37; N, 7.59; Cl, 4.80. Found: C, 68.36; H, 7.35; N, 7.52; Cl, 4.71. FAB MS (+ve mode): *m*/*z* 702, 379.

Synthesis of $[Fe\{(3,5\text{-}{}^tBu_2)\text{-salpm}\}_2]NO_3 \cdot 2H_2O$. This complex was produced in 69.8% yield as described for $[Fe\{(3,5\text{-}{}^tBu_2)\text{-salpm}\}_2]ClO_4$, with the exception that the salt used was $Fe(NO_3)_3 \cdot$

(34) Lanznaster, M.; Neves, A.; Bortoluzzi, A. J.; Assumpção, A. M. C.; Vencato, I.; Machado, S. P.; Drechsel, S. M. *Inorg. Chem.* **2006**, *45*, 1005.
(35) Shongwe, M. S.; Al-Hatmi, S. K. M.; Marques, H. M.; Smith, R.; Nukada, R.; Mikuriya, M. *J. Chem. Soc., Dalton Trans.* **2002**, 4064.

$9H_2O$. Slow evaporation of the purplish indigo solution at room temperature over a period of approximately one week afforded black diamond-shaped crystals of $[Fe\{(3,5\text{-}^tBu_2)\text{-salpm}\}_2]NO_3 \cdot 2H_2O$. Anal. Calcd for $[C_{42}H_{58}FeN_5O_7]$: C, 63.00; H, 7.30; N, 8.75. Found: C, 63.04; H, 7.28; N, 8.77. FAB MS (+ve mode): *m*/*z* 702, 379.

Acknowledgment. Financial support of this work was provided by Sultan Qaboos University (Grant IG/SCI/CHEM/07/04).

Supporting Information Available: Table of IR spectroscopic data for iron(III) complexes, packing diagram for $[Fe(salpm)_2]ClO_4$ at 100 K, electronic spectra of $[Fe(salpm)_2]ClO_4 \cdot 0.5EtOH$ and $Fe\{(3,5\text{-}^tBu_2)\text{-salpm}\}_2]ClO_4$, and CIF files of the complexes $[Fe(salpm)_2]ClO_4$ and $[Fe\{(3,5\text{-}^tBu_2)\text{-salpm}\}_2]NO_3 \cdot 2H_2O$. This material is available free of charge via the Internet at http://pubs.acs.org.

IC700397U